Thermodynamics of Mixed Stratocumulus Layers: Saturation Point Budgets

ALAN K. BETTS

West Pawlet, VT 05775

(Manuscript received 17 December 1982, in final form 6 July 1983)

ABSTRACT

Saturation point (SP) diagrams and a circulation model are used to analyze the thermodynamics of mixed stratocumulus layers, and develop conceptual tools for observational and parametric analyses. These models show the relation between SP structure and the thermodynamic fluxes for steady and unsteady mixed layers, couple convective and radiative fluxes at cloud top and within the layer, and suggest closure conditions on the circulation energetics using θ_v isopleths. The steady-state model shows a mixing line SP structure below cloud top with correspondingly simple surface flux parameterizations. The time-dependent mixed layer budgets are formulated using an SP vector diagram to show the approach to equilibrium, the internal circulation, and the relationship between Eulerian and Lagrangian flux descriptions.

1. Introduction

There has been extensive development of mixed layer models of stratocumulus which do not explicitly resolve the internal circulation of the layer (Lilly, 1968; Schubert, 1976; Schubert *et al.*, 1979a,b; Stage and Businger, 1981a,b), as well as numerical simulations which resolve a fully three-dimensional flow (Deardorff, 1976, 1980b). Randall (1980), Deardorff (1980a) and Moeng and Arakawa (1980) have analyzed cloud-top entrainment instability, and there have been several recent observational studies: Mahrt and Paumier (1982), Brost *et al.*, 1982a,b; Roach *et al.*, 1982; Caughey *et al.*, 1982; Slingo *et al.*, 1982. There is, however, much that remains unknown about the internal circulations within a stratocumulus layer: whether a single-cell cellular structure dominates or whether penetrative convection plays an important role. The radiative and convective fluxes and cloud-top entrainment are all closely coupled, but the questions of how this coupling should be modeled and what the scale is of circulations generated by radiative cooling of cloud top remain unresolved (Schubert *et al.*, 1979a; Kahn and Businger, 1979; Deardorff and Businger, 1980; Lilly and Schubert, 1980; Stage and Businger, 1981b), partly because of the lack of a model for the internal structure. It may be fruitful to contrast mixed-layer models for dry convection (Betts, 1973; Carson, 1973; Tennekes, 1973) and stratocumulus with parametric models for cumulus convection (Yanai *et al.*, 1973; Arakawa and Schubert, 1974; Betts, 1975). The introduction of convective mass transport to couple the fluxes of heat and moisture into subcloud-layer models (Betts, 1976) has proved useful in *observational* analyses of the structure of subcloud-layer fluxes (Nicholls and LeMone, 1980; Greenhut and Khalsa, 1982) and may play a similar role in clarifying the process in stratocumulus. Recently, Betts (1982a,b) showed how atmospheric convective structure and mixing processes and moist thermodynamics in general could be simplified using air parcel *saturation point.*

This paper attempts to integrate these ideas and develop a parametric model for a highly idealized internal circulation in a stratocumulus layer, in conjunction with a mixed-layer budget model formulated in the saturation point (SP) framework. In the process we shall develop certain important new concepts which have much wider applicability to mixed-layer models, convective budgets and atmospheric convection generally:

1) The SP notation gives a compact representation of atmospheric thermodynamic budgets.
2) SP circulation models give a clear physical model for the convective process, and relate Eulerian and Lagrangian descriptions of the mean fluxes and budgets.
3) The SP formulation describes the fluxes at the surface and the cloud-top inversion simply and elegantly.
4) The SP formulation describes the vertical structure of the fluxes of all the conserved parameters and the buoyancy flux in a single vector diagram.
5) Steady-state mixed layers attain a mixing line structure, while time-dependent layers can be analyzed in terms of their (vector) deviation from a mixing line structure.

These tools will be used to analyze the *thermodynamic* constraints on the structure and circulation in stratocumulus, and clarify some aspects of the role of cloud-top radiative processes and entrainment. This

paper is entirely theoretical (although some of the topics have already been described observationally in the literature), and the model chosen is the simplest possible one (single cell, constant mass flux, with radiative divergence only at cloud top—except in Section 5b). The intent, however, is to suggest procedures for stratifying and interpreting data sets (whether observational or simulated). It is possible that a range of stratocumulus circulations exist (different, for example, over warm and cold underlying surfaces) and that only some will fit the proposed simple mixed-layer model with constant mass flux. However, many of the concepts have general applicability, and will aid in unraveling mixing and radiative processes on different scales, as well as the bulk energetics of the whole stratocumulus layer. No attempt is made here to give complete prognostic solutions, nor to address the details of the turbulent process since it is clear that the energetics of entrainment deserves further observational study first.

2. Thermodynamic model for steady-state stratocumulus

a. Conceptual model

Schubert *et al.* (1979) and Betts (1978) presented conceptual parcel paths for the ascending and descending branches of the circulation inside a mixed stratocumulus layer. This paper combines Betts (1978) with the saturation point approach of Betts (1982a).

The reader should refer to Betts (1982a) for a full discussion of the saturation point (SP). In essence, the SP of an unsaturated (cloudy) air parcel is found by dry (moist) adiabatic ascent (descent) to the pressure level where a parcel is just saturated (with no cloud liquid water). At this saturation level (SL), parcel temperature and pressure (T_{SL}, p_{SL}) uniquely specify the conserved thermodynamic parameters. When two air parcels mix, the SP's of any mixture lie on mixing line joining the SP's of the two parcels. Radiative cooling changes a parcel SP at constant total water.

Stratocumulus is perhaps one of the simpler cloud systems, transporting heat and water between an underlying surface and the free atmosphere above, which is usually subsiding. We shall consider a horizontally homogeneous, initially steady-state, well-mixed layer (cloud and subcloud). This in itself imposes important thermodynamic constraints which can be explored using budget methods. The internal circulation will be modeled using a single cell with a constant convective mass circulation and ascending and descending branches (of equal areas, and each with distinct thermodynamic properties, that is, saturation points). In the circulation, cloud-top processes (mixing and radiation) modify the saturation point of ascending air to that of descending air, while the surface fluxes modify descending air back to ascending air. Fig. 1 schematically shows these processes. Points **A** and **D** denote the SP's of the ascending and descending branches,

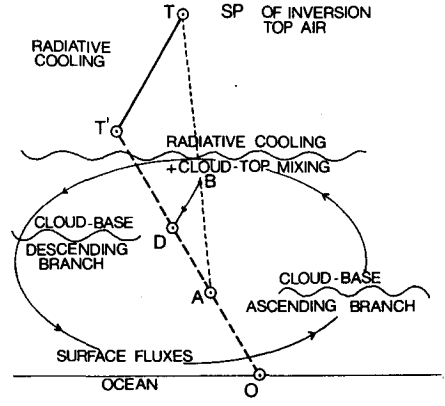

FIG. 1. Schematic for steady-state well-mixed stratocumulus over the ocean showing saturation point diagram and cloud bases for ascending and descending branches of a single-cell circulation.

respectively. At cloud top, the change of SP from **A** to **D** could be split conceptually into two processes: first, a mixing process which moves SP **A** to **B** up the mixing line (light dashes) toward the SP **T** of the sinking air above the cloud-top inversion (we shall suppose a sharp inversion at cloud top) and then a radiative cooling which moves the SP of the mixture at constant q_s from **B** to **D**. This splitting is conceptual and can be done in other ways. One may consider the inversion top air being cooled by radiation from **T** to **T'** as it sinks through the inversion and then being mixed with ascending air **A** to give the SP at **D**. This proves to be a useful concept and one we shall use here (see Section 2c). Fig. 9 shows another possible partition of the process. However radiational cooling and mixing are conceptually partitioned, we shall formally consider them to occur *together* at a sharp cloud-top interface. Section 5 discusses this modeling of cloud-top radiation in much greater detail.

At the surface, the change of SP from **D** to **A** results from the surface fluxes (see Section 2e). The saturation levels of **A** and **D** are the respective cloud bases for the ascending and descending branches (Betts, 1978).

The simplifications represented by this model (Fig. 1) should be clearly appreciated. We are not modeling penetrative convection, or the details of the cloud-scale turbulence; the effect of radiation has been treated only as a cloud-top process, and the assumption of a steady-state mixed layer (which implies a constant flux of the conserved parameters) between surface and inversion at cloud top, may be overrestrictive for some stratocumulus layers. The circulation is most likely in stratocumulus over a cold underlying surface, which is the case drawn in Fig. 1.

We shall first use budget equations for the steady-state stratocumulus layer, and then use saturation point diagrams to depict structure (and, indirectly, the fluxes) and explore considerations of buoyancy and entrainment. In Section 4, we relax the steady-state assump-

tion, and consider time-dependent mixed layers, to give a model of more general applicability.

b. Budget equations

The budget equation for a conserved thermodynamic parameter X can be written (e.g., Betts, 1975)

$$\frac{\partial \bar{X}}{\partial t} + \mathbf{V}\cdot\nabla\bar{X} + \omega\frac{\partial \bar{X}}{\partial p} = -\frac{\partial}{\partial p}\overline{\omega' X'} + S_X, \quad (1)$$

where S_X is a source term for X. If we consider a steady-state horizontally homogeneous, vertically well-mixed layer, then (1) reduces to

$$\frac{\partial}{\partial p}\overline{\omega' X'} = S_X. \quad (2)$$

The only source term we shall consider is a radiative flux divergence R_X, at a cloud-top inversion. Hence all fluxes $F_X = -\overline{\omega' X'} g^{-1}$ (defined positive for upward flux) are constant between the surface and inversion base. These fluxes can be represented three ways: at the two interfaces, and as a transport process in the mixed layer.

At the surface, using a bulk aerodynamic formula,

$$F_X = \bar{\omega}_0(\bar{X}_0 - \bar{X}_M)g^{-1}, \quad (3)$$

where $\bar{\omega}_0 g^{-1} = \rho C \bar{V}$, where $\bar{V}$ is the surface mean wind speed and the subscripts 0, M denote surface (not screen-level) and mixed-layer values. Here, C is a bulk aerodynamic transfer coefficient, which we shall assume is the same for all thermodynamic fluxes.

In the mixed layer, we shall parameterize the flux (e.g., Betts, 1978) by

$$F_X = \omega^* g^{-1}(\bar{X}_A - \bar{X}_D), \quad (4)$$

where $\omega^* g^{-1}$ is a cloud mass flux (positive), a measure of the intensity of the stratocumulus circulation, and the suffices A and D denote characteristic mean values for the ascending and descending branches of the circulation. For simplicity, we suppose both ascent and descent cover equal areas, so that

$$\bar{X}_M = (\bar{X}_A + \bar{X}_D)/2. \quad (5)$$

A constant flux in the mixed layer means that ω^*, $\bar{X}_A$, $\bar{X}_D$, are independent of height. In fact, ω^* remains a parameter which is never explicitly determined in the mixed-layer model, since it is the *fluxes* that are constrained.

At the cloud-top inversion, integration of the budget equation over the interface, which we suppose has infinitesimal depth, gives

$$F_X = \bar{\omega}_T g^{-1}(\bar{X}_M - \bar{X}_T) + R_X, \quad (6)$$

where, in the steady state, the entrainment velocity $\bar{\omega}_e = \bar{\omega}_T$, the mean subsidence at cloud top (suffix T denotes above cloud-top inversion). R_X is the radiative flux difference across the inversion (absent from the water budget).

Eqs. (3), (4) and (6) involve three characteristic "velocity" scales $\bar{\omega}_0$, ω^* and $\bar{\omega}_T$ (in p-coordinates: all positive here). If $\bar{\omega}_0$, $\bar{X}_0$, $\bar{\omega}_T$, $\bar{X}_T$ and R_X are externally specified, much of the thermodynamic structure of the mixed layer is determined [Schubert (1976) and Section 2e]. The internal circulation depends on the relative magnitude of ω^* to the external velocity parameters $\bar{\omega}_0$, $\bar{\omega}_T$. Eq. (6), when compared with (3) and (4), contains an extra term for the cloud-top radiative flux divergence, but this can be eliminated with a simple transformation, so that the fluxes (F_X) can be grasped conceptually on an SP diagram (Section 2g).

c. Radiative modification of cloud-top saturation point

Fig. 1 showed how the radiative flux divergence could be regarded as modifying the cloud-top SP from T to T'. This is a transformation of (6):

$$\begin{aligned} F_X &= \bar{\omega}_T g^{-1}(\bar{X}_M - \bar{X}_T) + R_X \\ &= \bar{\omega}_T g^{-1}(\bar{X}_M - \bar{X}_{T'}), \end{aligned} \quad (7)$$

where $\bar{X}_{T'}$ is the radiatively modified value at the SP T', given by

$$R_X = \bar{\omega}_T g^{-1}(\bar{X}_{T'} - \bar{X}_T). \quad (8)$$

The physical meaning of (8) is simple. The change in SP from T to T' is associated with radiative cooling, so that T T' is a line of constant q_s on a thermodynamic diagram. If we consider inversion top air sinking through the zone of strong radiative cooling at cloud top, its change of θ (or θ_L) is given along T T' by

$$\Delta\theta = \int S_\theta dt = \frac{1}{\bar{\omega}_T}\int S_\theta dp = gR_\theta/\bar{\omega}_T, \quad (8a)$$

where S_θ is the local radiative cooling rate of θ. We see that this modification is proportional to the radiative flux divergence of θ and inversely proportional to the subsidence. The change of θ and θ_E along with T T' are related, since q_s is constant [see also Betts, 1982a, (A10)] by

$$\Delta\theta/\theta = \Delta\theta_E/\theta_E, \quad (8b)$$

as are R_θ and R_{θ_E}.

d. Surface saturation point

The SP of surface air is also of crucial importance to the layer budgets. Over the ocean this is particularly simple if we assume surface air is just saturated at the ocean surface temperature, so that its SL (p_0) is also the surface pressure. Over land, the LCL corresponding to surface air properties (not screen-level) is the corresponding SP, which is typically well above the surface. Eq. (3) then involves the difference between the surface and mixed-layer SP's.

e. Parameterization of conserved fluxes

Since we are using thermodynamic diagrams for illustration of saturation points, we shall use potential temperatures here as conserved parameters, although for many budget purposes it is more convenient to use static energies, which are additive functions. [See Betts (1974) for a discussion of the different approximations involved.] Eqs. (3), (4) and (7) represent the same fluxes as three different parameterizations, involving three velocity scales and three thermodynamic differences:

$$gF_\theta = \bar{\omega}_0(\bar{\theta}_0 - \bar{\theta}_M) = \omega^*(\bar{\theta}_A - \bar{\theta}_D) = \bar{\omega}_T(\bar{\theta}_M - \bar{\theta}_{T'}), \quad (9a)$$

$$gF_{\theta_E} = \bar{\omega}_0(\bar{\theta}_{E_0} - \bar{\theta}_{EM}) = \omega^*(\bar{\theta}_{EA} - \bar{\theta}_{ED}) = \omega_T(\bar{\theta}_{EM} - \bar{\theta}_{ET'}), \quad (9b)$$

$$gF_q = \bar{\omega}_0(\bar{q}_0 - \bar{q}_M) = \omega^*(\bar{q}_A - \bar{q}_D) = \bar{\omega}_T(\bar{q}_M - \bar{q}_{T'}). \quad (9c)$$

All parameters are SP values. For brevity no further subscripts are introduced here but, for example, θ represents saturation level θ_{SL} and hence potential temperature θ for unsaturated air (below its SL) and liquid water potential temperature θ_L for cloudy air (Betts, 1982a). Note also that $q_{T'} = q_T$.

To good approximation, a similar equation can be written for the flux of saturation pressure difference ($\mathcal{P} = p_{SL} - p$). Mathematically this may be regarded as another linear combination of say (9a) and (9c). (See Appendix A.) Its physical meaning is that a convergence of the flux $\overline{\omega'\mathcal{P}'}$ tends to bring the layer toward saturation, i.e.,

$$gF_{\mathcal{P}} = \bar{\omega}_0(p_0 - p_M) = \omega^*(p_A - p_D) = \bar{\omega}_T(p_M - p_{T'}). \quad (9d)$$

Again, these are all saturation level pressures: p_A, p_D, correspond to cloud base for the ascending and descending branches respectively, and $p_M = (p_A + p_D)/2$ to mean cloud base. Over the ocean, p_0 is just the surface level pressure, so it is clear that this equation gives a particularly simple visualization of the balance of the structure and fluxes mostly in terms of observable pressures.

f. Vector representation of fluxes using SP

Eqs. (3), (4), (6), (8) and (9) all involve fluxes expressed as the product of a velocity scale and the difference of sets of conserved thermodynamic parameters, which means the difference of pairs of saturation points, since each SP defines a set of conserved thermodynamic parameters. It is convenient to use a vector notation for SP's; we shall write the difference of 2 SP's as

$$(\mathbf{A} - \mathbf{B}) \equiv (\mathbf{X}_A - \mathbf{X}_B).$$

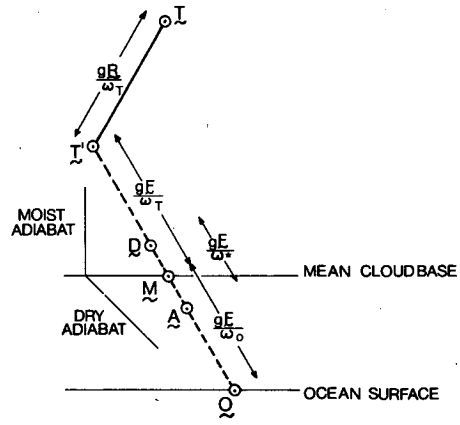

FIG. 2. Schematic saturation point diagram for steady-state stratocumulus over the ocean. The heavy dashed line is a mixing line. TT' is the radiative modification of inversion-top SP along a line of constant q_s. The relation between fluxes and SP differences are as shown.

The SP corresponding to **A** is uniquely defined (on a thermodynamic diagram, for example, Fig. 2) by any *two* of the coordinates (p_{SL}, θ_{SL}, θ_{ESL}, q_{SL}). This greatly simplifies the notation. Eqs. (9) and (8) become (dropping the overbars)

$$g\mathbf{F} = \omega_0(\mathbf{0} - \mathbf{M}) = \omega^*(\mathbf{A} - \mathbf{D}) = \omega_T(\mathbf{M} - \mathbf{T}'), \quad (9')$$

with

$$\omega_e = \omega_T,$$

and

$$g\mathbf{R} = \omega_T(\mathbf{T}' - \mathbf{T}), \quad (8')$$

where we have denoted the convective flux vector by **F**, and the radiative flux difference at cloud top by **R** (which is a vector at constant q_s on a thermodynamic diagram—see Section 2h). The full power of this notation will become evident in Section 4, where unsteady layers are considered.

g. Solution of constant flux equations

Solving (9') for the mixed layer SP **M** (Schubert, 1976) gives

$$\mathbf{M} = \frac{\omega_0\mathbf{0} + \omega_T\mathbf{T}'}{\omega_0 + \omega_T}. \quad (10a)$$

Parallel expressions exist in terms of **A**, **D** and ω^*, e.g.

$$\mathbf{M} = \frac{2\omega^*\mathbf{A} + \omega_T\mathbf{T}'}{2\omega^* + \omega_T} = \frac{2\omega^*\mathbf{D} + \omega_0\mathbf{0}}{2\omega^* + \omega_0}. \quad (10b)$$

More complex expressions can be extracted for the SP's of ascending and descending branches, e.g.,

$$\mathbf{A} = \frac{\omega_0\mathbf{0} + (2\omega^* - \omega_0)\mathbf{M}}{2\omega^*} = \frac{(1 + \omega_T/2\omega^*)\omega_0\mathbf{0} + (1 - \omega_0/2\omega^*)\omega_T\mathbf{T}'}{\omega_0 + \omega_T}. \quad (11)$$

It is clear that with the constant flux assumption (steady-state) and the representation of the cloud-top radiative divergence as a single modification of inversion top air (T to T′), SP's within the mixed layer are then simple averages (weighted by combinations of the characteristic velocities) of the end points **0**, **T**′. It follows that the four SP's **0**, **A**, **D** and **T**′ lie on one *mixing* line, and that processes within the mixed layer can be represented diagrammatically as mixing processes.

h. Parameterization of surface fluxes

Another rearrangement of (9′) gives the surface fluxes in terms of differences across the layer:

$$g\mathbf{F} = \left(\frac{\omega_T\omega_0}{\omega_T + \omega_0}\right)(\mathbf{0} - \mathbf{T}'), \tag{12}$$

which represents the surface fluxes of θ, q, θ_E and $\mathcal{P}$. Specifically the sensible and latent heat fluxes are found from

$$gF_\theta = \left(\frac{\omega_T\omega_0}{\omega_T + \omega_0}\right)(\theta_0 - \theta_T), \tag{12a}$$

$$gF_q = \left(\frac{\omega_T\omega_0}{\omega_T + \omega_0}\right)(q_0 - q_T). \tag{12b}$$

Note that (12a) implicitly contains the cloud-top radiation, which cools **T** to **T**′, but (12b) does not, since $q_T = q_{T'}$.

Thus, the determination of the surface fluxes, for the steady-state stratocumulus layer, requires surface parameters ω_0 ($=\rho g C \bar{V}_0$), **0** (the SP of surface air), and a set of cloud-top parameters, **T**, ω_T and **R** (which determine **T**′ through (8′).

i. SP diagram of constant flux structure

The mixing line structure (Section 2g) and the implicit equations (8′), (9′), (10) and (11) can be shown graphically on a thermodynamic diagram (Fig. 2).

The cloud-top radiative modification (8′) is along a line of constant q_s: the spacing of **T** **T**′ is inversely related to ω_T ($=\omega_e$). The vector separation of the SP's **0**, **A**, **D**, **T**′ along the mixing line (heavy dashed) is related to the mixed layer fluxes (9′) as shown. These SP difference vectors and fluxes can be projected onto any of the coordinates axes of the diagram. For example, the pressure difference of SP's are related to the flux $F_\mathcal{P}$ [through (9d)].

The θ, q, θ_E differences satisfy (9a), (9b) and (9c), respectively. This diagram and the equations it represents consolidate a great deal of information, and several conclusions can be summarized.

1) Steady-state mixed layers attain a mixing line thermodynamic structure. Given the SP's of surface and inversion-top air, the radiative flux difference **R**, the characteristic velocities $\bar{\omega}_0$ and $\bar{\omega}_T$, the general thermodynamic structure of a steady-state horizontally homogeneous stratocumulus layer is determined: specifically, mean-layer properties, mean cloud base and mean fluxes. From an observational viewpoint, we would expect SPs of all air within the layer to be on this mixing line in the steady state.

2) The surface fluxes can be formulated as a mixing process between surface air and mixed-layer air (using the same surface transfer coefficient for all thermodynamic processes). They can also be expressed in terms of thermodynamic differences across the whole layer (12), for the steady-state case.

3) Cloud-top processes can be described as a radiative process together with a mixing process. Fig. 2 couples radiative and convective thermodynamic processes in one diagram. This permits discussion of the role of the processes in the energetics of the layer (see later sections).

4) The internal mass circulation ω^* and correspondingly, the difference **A** − **D** [related through (9)] between ascending and descending branches of the circulation is *not determined* directly by these external parameters and, in fact, need not be determined in a simple prognostic model (see Section 2j). However, ω^* is constrained because **A**, **D** fall on the mixing line, and are bounded by **0**, **T**′. As the circulation ω^* slows down, the difference (**A** − **D**) increases. Eq. (12) shows that **A** approaches **0** as $2\omega^* \rightarrow \omega_0$. Similarly, **D** approaches **T** as $2\omega^* \rightarrow \omega_T$. Thus we require

$$2\omega^* > \omega_0, \omega_T.$$

If ω^* decreases, the difference between ascending and descending branch cloud base increases, and the cloud layer will break up if **D** reaches cloud top (which Fig. 2 does not show). For the unsteady case (Section 4), we shall find that a well-mixed layer requires an internal circulation ω^* which is fast compared to $(\omega_0 + \omega_T)$.

5) The slope of the mixing line **0** **T**′ which is controlled by the external parameters **0**, **T**, **R**, ω_T is important. It apparently determines, for example, the temperature and moisture difference between surface and mixed layer [whether $\theta(\mathbf{0}) \lesseqgtr \theta(\mathbf{M})$]; in fact, we shall find in Sections 3 and 4 that the case with a warm surface is unsteady. However, the slope of the mixing line **0**, **T**′ is fundamental to the energetics of the layer (see Section 3).

6) Closure is a little implicit in Fig. 2. We shall see in Section 3b that the energetic constraints on the slope of the mixing line **0** **T**′, are sufficient to fix **T**′ and the cloud-top equilibrium height is that for which **T**′, **T**, ω_T, **R** satisfy (8′).

7) From an observational viewpoint, the characteristic velocities ω_0, ω^*, ω_T are related to four saturation level pressures through (9d): p_0 (here ocean surface pressure), p_A, p_D and hence, p_M (the cloud bases for the ascending and descending branches and their mean) and $p_{T'}$, which is derived from p_T using (8′). Three (p_0, p_A, p_D) are observable, so that given ω_0, it is observationally possible to compute ω^* from (9d).

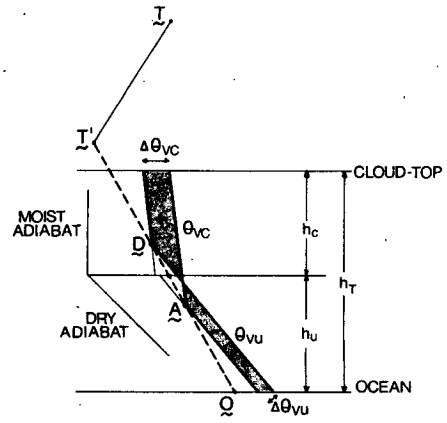

FIG. 3. Construction of convective available potential energy (shaded area) using θ_v isopleths through SP's of ascending and descending branches for steady-state stratocumulus over a (cold) ocean. Mixed layer depth is h_r; h_c and h_u are the mean pressure thicknesses for the cloud and subcloud (unsaturated) layers respectively.

p_T can be computed from observations, so that also given **R**, one can iterate to find **T**′, and ω_T using (9d) and (8′).

j. Buoyancy, θ_v fluxes and convective available potential energy (CAPE)

Betts (1982a) showed how θ_v isopleths (θ_{vc} for cloudy air and θ_{vu} for unsaturated air) could be added to SP thermodynamic diagrams to discuss buoyancy and convective available potential energy (CAPE). Appendix B summarizes and extends this analysis by defining a θ_{ESV} corresponding to θ_{vc}. The construction for the constant flux stratocumulus layer is shown in Fig. 3. As in Fig. 2, **0ADT**′ is the mixing line. Isopleths θ_{vu}, $\theta_{vc}(\theta_{ESV})$ are drawn through **A**, **D**, the SP's of the ascending and descending branches of the circulation. These θ_v isopleths are used to compare θ_v differences just as the θ, θ_{ES} isopleths would be used to compare differences of θ, or θ_{ES}. Above **D**, both branches of the circulation are cloudy and **A** has positive buoyancy; below **A**, both are unsaturated and **D** has greater buoyancy.

This construction is the projection of the SP's onto the θ_v isopleths and we shall use the notation for the parcel differences

$$(\mathbf{A} - \mathbf{D})_{\theta_{vc}} \equiv \Delta\theta_{vc}, \tag{13a}$$

$$(\mathbf{A} - \mathbf{D})_{\theta_{vu}} \equiv \Delta\theta_{vu}. \tag{13b}$$

Fig. 3 is a schematic drawn for an arbitrary (**A** − **D**), since neither (**A** − **D**) nor ω^* are determined separately in this simple prognostic model. Their product, however, which is related to the buoyancy *flux*, and is a projection of the flux **F**, is subject to energetic constraints (see below). The criterion for no cloud-top entrainment instability (Randall, 1980; Deardorff, 1980a) is that **A T** lies to the right of the θ_{vc} isopleth (Betts, 1982a). In Section 5b we generalize the criterion to include radiative cooling. This criterion is satisfied in Fig. 3, so that cloud-top mixing alone does not produce freely entraining negatively buoyant downdrafts. Instead, there is a slower circulation in which cloudy mixtures become negatively buoyant at cloud top by radiative cooling. This is represented by the radiative cooling of **T** to **T**′, together with mixing to give **D**. For a direct thermal circulation in the cloud layer (driven, that is, by radiative cooling), we require the mixing line **0ADT**′ to lie to the left of the θ_{vc} isopleth through **A**, so that $\Delta\theta_{vc}$ is positive as shown. Conversely, in the subcloud layer (below **A**), Fig. 3 shows $\Delta\theta_{vu}$ negative, which means the ascending branch has negative buoyancy and the subcloud circulation is (in the case shown) an indirect one driven by the available potential energy converted in the cloud layer. Since the circulation as a whole must be energy generating, there is a constraint on $\Delta\theta_{vc}$, $\Delta\theta_{vu}$ and the slope of **0ADT**′.

The shaded area times ω^* is (closely) the convective available potential energy for the circulation (the integral of the buoyancy flux) $F_{\theta_v} = \omega^*(\mathbf{A} - \mathbf{D})_{\theta_v}/g^{-1}$; see Appendix B. The light construction lines show that this shaded area is exactly equivalent to treating both parcels as cloudy above mean cloud-base **M** and unsaturated below. Hence, we do not need to consider in detail the region between p_A and p_D, which is undefined as long as the magnitude of ω^* is undefined. The net CAPE is then (in flux form)

$$\text{CAPE} = \frac{\bar{\rho}\omega^*}{g\bar{\theta}_v}(h_c\Delta\theta_{vc} + h_u\Delta\theta_{vu}), \tag{14}$$

where h_c, h_u are pressure thicknesses (Fig. 3). Since the buoyancy fluxes $\omega^*\Delta\theta_{vu}$, $\omega^*\Delta\theta_{vc}$ are determined by the flux **F** (see Section 2b), although neither ω^* nor (**A** − **D**) are determined separately, so is CAPE determined for constant h_c, h_u. Eq. (14) has another relationship through the slope of the mixing line to the concepts of maximum and minimum entrainment (Lilly, 1968; Schubert, 1976). (See Section 3b.)

k. Flux structure of steady-state mixed layer

Fig. 4 summarizes the fluxes of the conserved parameters (solid lines) for the steady-state mixed layer,

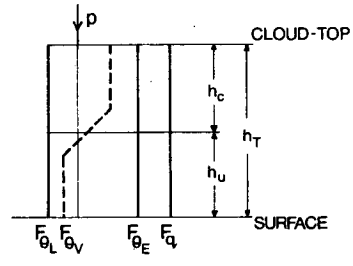

FIG. 4. Fluxes of conserved parameters (solid lines) and θ_v (dashed lines) for steady-state mixed stratocumulus layer.

as well as the θ_v flux (dashed). Each can be regarded as a *projection* of the SP difference (**A** − **D**) onto a set of isopleths, multiplied by the mass circulation. For example,

$$gF_{\theta_L} = \omega^*(\mathbf{A} - \mathbf{D})_{\theta_L}.$$

The fluxes of θ_L, θ_E, q_T are constant and almost seem trivial; the flux of θ_v is more complex as there is a transition from the subcloud to cloud layers (Fig. 3). The important conceptual point is that the SP diagram, plus the velocity scales, gives the structure of *all* the convective fluxes. This remains true in the more complex unsteady case (see Figs. 5, 6). If desired, the fluxes of sensible and latent heat, and liquid water can also be separated.

3. Constraints on stratocumulus fluxes

a. θ budget over a cold surface

For stratocumulus over a cooler underlying surface, the downward surface flux of sensible heat is much smaller than the radiative flux difference at cloud top, i.e.,

$$F_\theta \ll R_\theta,$$

so that to first approximation from (9a)

$$\theta_{T'} \approx \theta_M \approx \theta_0, \tag{15}$$

which means that the mixing line between the surface SP and the radiatively modified SP **T**′ is closely a dry adiabat. Hence, from (8a) and (15)

$$\omega_e = \bar{\omega}_T \approx R_\theta/(\theta_T - \theta_0), \tag{16}$$

so that the entrainment and subsidence at cloud top can be estimated from the radiative flux divergence and the θ difference between surface and inversion top. If there is constant divergence so that the subsidence increases with height, then cloud top will in the steady state be at the height where (16) is satisfied. Schubert (1976) gave essentially the same equation for his minimum entrainment case using virtual potential temperature in (15) and (16). In this case, the mixing line is a θ_{vu} isopleth. This gives a slightly better approximation. Using either θ or θ_v gives a first-order parameterization for the surface fluxes. For example, using θ, Eq. (12a) gives $F_\theta = 0$ and Eq. (16) can be solved iteratively in a numerical model to find a consistent set of $\bar{\omega}_T$, θ_T, R_θ. Then (12b) gives F_q and (10), q_M: This may be regarded as a parameterization of a passive stratocumulus layer, which is transporting latent but not sensible heat. It is driven by cloud-top cooling, where there are two large terms in the sensible heat flux budget which balance [Eq. (8a)].

b. Closure condition on CAPE

There has been considerable discussion of an appropriate closure condition on the KE budget of an entraining mixed layer. Ball (1960) realized that convective overshoot in a dry mixed layer heated from below could drive entrainment and a downward heat flux at the top of the mixed layer and suggested a simple closure. Lilly (1968) applied the idea to stratocumulus and subsequently this closure model was applied in different forms to dry mixed layers (Betts, 1973; Carson, 1973; Tennekes, 1973) and stratocumulus (Schubert, 1976; Deardorff, 1976; Kraus and Schaller, 1978; and others). Stage and Businger (1981a,b) discuss these models at length, and following Manins and Turner (1978), attempt to partition the buoyancy flux so as to distinguish between production terms in the KE budget (e.g., surface heat flux if upward, cloud-top radiative cooling) and consumption terms (e.g., cloud-top entrainment of warm air). From the perspective of our circulation model, this partition does not seem realistic (see Section 4g), and we shall consider closures based simply on the circulation kinetic energy budget.

The energy available to drive the stratocumulus circulation in this steady-state case depends critically on the slope of the mixing line **0ADT**′ in relation to the θ_{vu}, θ_{vc} isopleths [Fig. 3 and Eq. (14)]. If **0T**′ is parallel to the θ_{vu} isopleth there is zero KE generation in the subcloud layer, and larger generation in the cloud layer; this might be regarded as *minimum* entrainment (Lilly, 1968) since ω_e is minimized; CAPE is maximized in (14) as

$$\Delta\theta_{vu} = 0.$$

As the slope **0T**′ increases toward that of the θ_{vc} isopleth, the negative subcloud contribution to CAPE increases, while the positive cloud layer contribution decreases, until the total CAPE in (14) is zero; this might be regarded as *maximum* entrainment (**TT**′ is minimized, ω_e maximized); therefore,

$$\frac{\omega^*}{\bar{\theta}_v}(h_c\Delta\theta_{vc} + h_u\Delta\theta_{vu}) = 0. \tag{14′}$$

Realistically, we would expect the circulation to be able to drive some region of negative energy flux (and negative KE generation) but not approach (14′) because of KE dissipation. If δ is the fraction of the KE generated that is dissipated, we could define an intermediate closure by

$$\frac{h_u\Delta\theta_{vu}}{h_c\Delta\theta_{vc}} = 1 - \delta, \tag{17}$$

which is independent of ω^*, and the magnitude of (**A** − **D**). Estimates of δ vary from 0.8 to 0.99 (Stage and Businger, 1981b).

It is clear that if $1 - \delta$ is small, then the mixing line will be close to the θ_{vu} isopleth and the simple steady-state solutions discussed in (3a) will apply. In general, (17) fixes the slope of the mixing line **0T**′ and hence **TT**′. This fixes a value of $\omega_e = \omega_T$, using (8′) and **R**,

and a corresponding steady-state height. This formally closes the steady-state mixed layer model.

Conversely, an *observational* determination of the slope of the mixing line from measurements in a stratocumulus layer gives an estimate of δ from (17). This is a bulk approach to the estimation of δ, which may in general depend on a variety of factors including wind shear, horizontal scales of the circulation and turbulent structure, relative magnitude of surface heat flux, and cloud top radiative fluxes and many others.

A discussion of the more complex but more realistic unsteady layer follows in Section 4.

c. *Stratocumulus over a warm surface*

These arguments for the structure of the circulation seem convincing until stratocumulus over a warm surface is considered. Here, if the steady-state model were valid, $\theta_{T'}$ would be to the left of the θ_{vu} (and probably θ) isopleth in Fig. 3, so that the surface virtual heat flux is upward. What then happens to the entrainment condition associated with kinetic energy generation by the circulation? The θ_v flux is up at all levels, and it seems likely that this will increase the cloud-top entrainment.

The difficulty lies in the steady-state assumption. Over a warm surface a stratocumulus layer is being driven energetically by both the surface heat flux and cloud-top radiational cooling. Since it is unlikely that this is a steady-state, we next look at unsteady saturation point models for well-mixed layers.

4. Unsteady mixed layers

In this section, the steady-state assumption, which means fluxes independent of height, is relaxed. This introduces a new class of models for time-dependent mixed layers which have general applicability to dry mixed layers (which will be discussed in detail elsewhere) as well as stratocumulus. The full usefulness of the SP diagram as a *vector* diagram will become apparent (Section 4a). Furthermore, the time-dependent circulation model developed in Section 4c illustrates clearly the important conceptual relationship between Eulerian and Lagrangian flux descriptions.

a. *SP vector diagram for unsteady mixed layer*

The SP vector diagram can be used to describe the approach to equilibrium of a time-dependent layer (**M** not constant). The mixed layer budget equation can be written

$$h_T \frac{d\mathbf{M}}{dt} = \omega_0(\mathbf{0} - \mathbf{M}) - \omega_e(\mathbf{M} - \mathbf{T}'), \qquad (18)$$

where h_T is the pressure depth of the mixed layer (surface to cloud top), and the entrainment velocity at cloud top satisfies

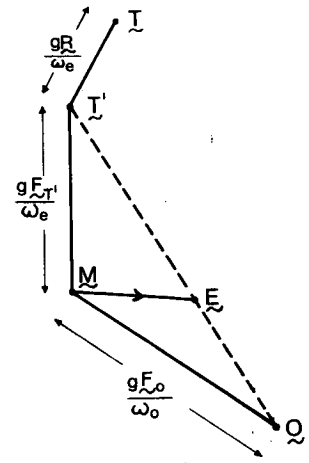

FIG. 5. Saturation point vector diagram for unsteady mixed stratocumulus layer. The mixed layer SP, M, has an (instantaneous) tendency towards E on the dashed mixing line between **0T'**.

$$\omega_e = \frac{dh_T}{dt} + \omega_T. \qquad (19)$$

The radiative flux divergence at cloud-top still satisfies (8′).

If we now define an equilibrium state **E** by

$$0 = \omega_0(\mathbf{0} - \mathbf{E}) - \omega_e(\mathbf{E} - \mathbf{T}'), \qquad (20)$$

then subtracting the vector equations (18) and (20) gives

$$h_T \frac{d\mathbf{M}}{dt} = (\omega_0 + \omega_e)(\mathbf{E} - \mathbf{M}). \qquad (21)$$

Eq. (21) expresses the tendency of the layer mean SP in terms of an SP difference from equilibrium (**E** − **M**) and an *adjustment time scale* for the *layer*, i.e.,

$$\tau = h_T/(\omega_0 + \omega_e). \qquad (22)$$

Fig. 5 shows the SP vector diagram. If the end-points **0**, **T**′ and ω_0, ω_e remain constant, then the layer will actually approach equilibrium at **E** (to give a steady-state solution on the mixing line **0 E T**′ discussed in Sections 2 and 3). Over the ocean, ignoring advection, ω_0, **0** might be considered constant in some cases,but in general, **T**, **T**′ will change as h_T, the mixed layer depth, changes. In this case, Fig. 5 is only an instantaneous diagram.

b. *Thermodynamic fluxes*

Fig. 6 shows as heavy solid lines the linear change of the fluxes of the conserved parameters from the surface to the inversion base (cloud top). Both Figs. 5 and 6 represent Eq. (18) in different ways.

In terms of the SP vector differences, the surface and inversion base fluxes in Fig. 6 can be regarded as projections of $\omega_0(\mathbf{0} - \mathbf{M})$ and $\omega_e(\mathbf{M} - \mathbf{T}')$, respectively,

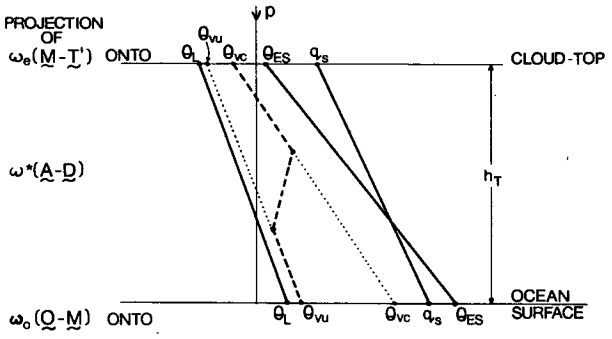

FIG. 6. Fluxes of conserved parameters (heavy solid lines) and θ_v (heavy dashed lines) for the unsteady mixed layer. Dotted lines are construction lines for θ_v fluxes.

onto the θ, θ_E and q_s coordinates for the θ_{SL}, θ_{ESL} and q_{SL} fluxes, respectively.

The heavy dashed line is the θ_v flux which has a more complex structure (discussed in Section 4d); it involves the projection of the SP differences onto the θ_{vu} isopleths for the unsaturated parcels and the θ_{vc} isopleths for cloudy parcels.

Viewing Figs. 5 and 6 together and supposing that ω_0, **0**, ω_e and **T**′ are *constant*, we can see that if cold dry air blows over a warm ocean initially, **M** is cooler and drier than the equilibrium state **E**, which **M** approaches. The surface fluxes $\omega_0(\mathbf{0}-\mathbf{M})$ are initially enhanced and decrease with time, while the inversion base convective flux $\omega_e(\mathbf{M}-\mathbf{T}')$ increases with time until, as $\mathbf{M}\rightarrow\mathbf{E}$, the steady state is reached with a constant flux through the mixed layer.

c. *Time-dependent circulation model*

Fig. 6 can be constructed from the surface and inversion-base fluxes and the mixed layer assumption, or viewed as another representation of Fig. 5, but clearly the linear change of the fluxes with height must imply an internal circulation with time-dependent ascending and descending branches. The SP diagram for this time-dependent circulation is of great importance conceptually and is shown in Fig. 7.

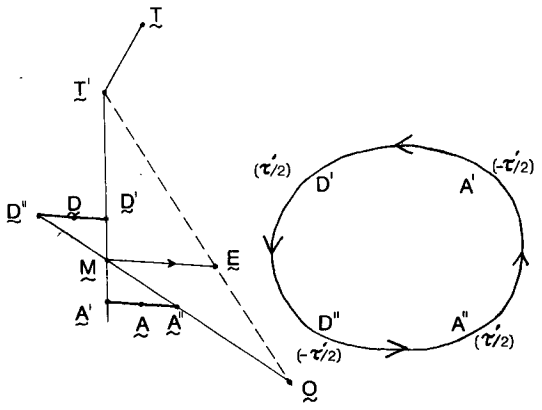

FIG. 7. As in Fig. 5, but showing instantaneous SP's for time-dependent internal circulation in unsteady stratocumulus (see text).

For simplicity we shall take **0**, ω_0, **T**′ and ω_e as constant, so that the trend of the layer mean is along **ME**. The trend with *time* at any height of ascending and descending air SP's is **A′AA″** and **D′DD″** parallel to vector **ME**. Just as **ME** is associated with a layer time-scale τ (22), so **A′AA″**, **D′DD″** are associated with τ', half the *circulation time scale*

$$\tau' = h_T/2\omega^*. \tag{23}$$

Here, τ' is the mean rise (sink) time from top to bottom of the layer in the ascending (descending) branch. For simplicity we shall still assume a mass circulation ω^* independent of height (except very close to the top and bottom boundaries), since this is sufficient to represent the fluxes [see (24)]. The mixed layer assumption requires a fast circulation; that is $\tau' \ll \tau$ or $2\omega^* \gg (\omega_0 + \omega_e)$ (geometrically this corresponds to $|\mathbf{AD}| \ll \mathbf{ME}$), so that the change $d\mathbf{M}/dt$ is small as air ascends from top to bottom of the layer. It then follows that the SP of air in each branch changes linearly with height (from **A″** to **A′**, and **D″** to **D′**).

Fig. 7 has both Eulerian and Lagrangian interpretations. Viewed as an instantaneous diagram from an Eulerian viewpoint, there is a flux gradient within the layer associated with a gradient of SP with height on the ascending and descending branches. At the surface

$$\omega^*(\mathbf{A}''-\mathbf{D}'') = \omega_0(\mathbf{0}-\mathbf{M}), \tag{24}$$

while at cloud top,

$$\omega^*(\mathbf{A}'-\mathbf{D}') = \omega_e(\mathbf{M}-\mathbf{T}'). \tag{24'}$$

A constant mass circulation ω^* will be assumed, leaving the linear gradient of the fluxes with height associated entirely with a linear change of $(\mathbf{A}-\mathbf{D})$ with height.

From a Lagrangian viewpoint parcel SP is conserved as air circulates, but because of the time dependence, air at different levels has different SP's. The schematic on the right of Fig. 7 shows the location of air in the circulation with different properties. The surface transformation of SP is from **D″** to **A″** on the mixing line **0A″D″** and the cloud-top transformation is from **A′** to **D′** on the mixing line **T′D′A′**. The *opposite* gradients with height (for the ascending branch, **A″A′**; descending branch, **D″D′**) can be understood from the time dependence. If we take a reference time zero as air passes the midpoint of the layer with midpoint properties $\hat{\mathbf{A}}\hat{\mathbf{D}}$, then in the Lagrangian frame we can affix time labels to **A′**, **A″**, **D′**, **D″** as shown. For example, $(-\tau'/2)$ means that **A′**, **D″** air both passed the layer midpoint at the same past time: $-\tau'/2$. In this time frame, the cloud-top transformation is from **A′** $(-\tau'/2)$ to **D′** $(+\tau'/2)$, the converse at the surface.

To summarize, the importance of Fig. 7 in the study of atmosphere mixed layers lies in fact it relates Eu-

lerian and Lagrangian descriptions of the fluxes in an unsteady layer. Eq. (18) and Fig. 6 are Eulerian flux descriptions. Fig. 7 is both: it follows parcels whose SP's do not change as they ascend (descend) the layer. It also shows how the instantaneous fluxes change with height because the SP's at any level are time-dependent, and ascending and descending branches have opposite instantaneous vertical structures. For example, if the layer mean θ_E is increasing with time, then instantaneously θ_E will decrease (increase) with height in the ascending (descending) branches. Although a mixed layer is an idealization, great care must be taken with real atmospheric data not to confuse the instantaneous Eulerian picture (e.g., SP changes with height in ascending branch) with the Lagrangian circulation picture (SP does not change with height).

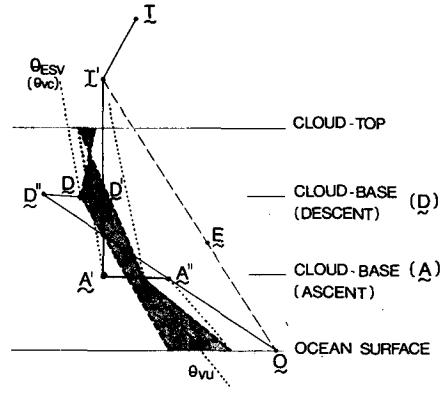

FIG. 8. Addition of θ_v isopleths (dotted lines) to Fig. 7 showing buoyancy and convective available potential energy (shaded area) for unsteady stratocumulus circulation.

d. Buoyancy flux and CAPE

The fluxes of the conserved parameters change linearly with height in the mixed layer, but the θ_v flux is more complex since the layer is partly cloudy and partly unsaturated. The θ_v flux structure (shown also in Fig. 6) can, however, be easily found by adding the θ_{vu}, θ_{vc} isopleths to Fig. 7, and projecting **A**, **D** onto them. Fig. 8 shows the construction: the heavy dashed lines are the paths of $\theta_v(p)$ for the ascending and descending branches; the dotted lines are θ_v isopleths. The θ_v flux is

$$\omega^*[\theta_v(\mathbf{A}, p) - \theta_v(\mathbf{D}, p)]/g.$$

The changing SP's **A**, **D** lead to changing θ_v differences with height with discontinuities of slope at the instantaneous cloud bases for ascending and descending branches. (Note that these are now changing with time and in general are not at the midpoints **A'A"**, **D'D"**.) In Fig. 8 the ascending branch has greater buoyancy than the descending branch at the surface (where the fluxes of θ and q are upward) but the difference decreases by the cloud-base level of **A**. Between **A** and **D** there is a transition, since ascending air is cloudy and descending air unsaturated. By the level of **D** the ascending air has increased its positive buoyancy. However, because of the continual trend of SP's (**D"D'** and **A"A'**) with height, the buoyancy flux becomes negative below cloud top. Fig. 8 shows an illustrative structure; the detailed structure will depend on the instantaneous **0**, **M**, **T'** and on some physical (closure) constraint on the buoyancy flux integral (see Section 4g). For example, the buoyancy flux might go negative just below cloud base in some cases.

Fig. 8 (and Fig. 6) have been drawn with net positive CAPE (the buoyancy flux integral), but the circulation as a whole is (in the case shown) able to drive a small region of negative flux, below cloud top. This flux structure follows from the SP structure for this mixed-layer model because the gradients of SP within the layer have adjusted to satisfy the time-dependent budgets. If there is some constraint on the buoyancy flux integral that must also be satisfied, then this imposes a constraint on **T'** and ω_e, which controls the entire SP structure given instantaneous values of ω_0, **0**, **M**, h_T (see Section 4f).

e. Cloud-top instability criteria: Time dependent layer

It is clear from Fig. 8, that in a stratocumulus layer which is moving toward warmer equilibrium temperatures, the stability of the layer as measured by the SP gradient (**A"D"**, **AD**, **A'D'**) increases markedly with height. In Fig. 8, a mean cloud layer value of $\overline{\mathbf{A} - \mathbf{D}}$ does meet the instability criteria, while at cloud top (**A'** − **D'**) is stable to cloud-top entrainment. Thus, for this unsteady layer, the mean gradient (**M** − **T'**) is not to the left of the θ_{vc} isopleth. But the case shown is only illustrative. The exact structure will depend on the relative contributions of the cloud and subcloud layers to the positive buoyancy flux integral.

f. Time-dependent solution

The graphical solution of the time-dependent case, including the structure of all the fluxes and general form of the SP diagram (everything, in fact, except the magnitude of ω^*) follows, once ω_e, **T'** are known. As in the steady-state case, these satisfy

$$\omega_e(\mathbf{T} - \mathbf{T}') = g\mathbf{R}, \tag{25}$$

where now $\omega_e = \omega_T + dh_T/dt$. If at any time **0**, **M**, **T**, ω_0, ω_T, h_T and **R** are specified, the prognostic problem is that of finding ω_e, **T'** to satisfy (25), which then gives the time dependence of all variables including dh_T/dt from (19), the deepening of the cloud layer.

As ω_e increases, **T'** approaches **T** and the layer fluxes change correspondingly. The net CAPE for the circulation decreases as ω_e increases because

1) As **T'** → **T**, the cloud-top θ_v flux becomes increasingly negative once **T'** crosses the θ_{vc} isopleth

through M. (For no cloud-top entrainment instability, T must be on the stable side of this isopleth.)

2) As ω_e increases, E $\rightarrow$ T′ (Fig. 7) and both cloud and subcloud layers become in the mean more stable, with reduced CAPE. It is clear that a condition on the CAPE closes the time-dependent problem.

g. Closure condition on CAPE

Stratocumulus over a warm surface is being driven by both surface heating and cloud-top cooling. Following the discussion of Section 4d, it seems likely that entrainment will increase until there are some (driven) regions of negative θ_v flux. This is likely to be possible at cloud top (see Section 4f) because T lies to the right of the θ_{vc} isopleth for no cloud-top entrainment instability, so as ω_e increases, T′ can approach T. If the subcloud layer is deep and the surface heat flux not too large, a negative θ_v flux will develop first at the top of the subcloud layer as T′ approaches T. This negative flux cannot become too large or the cloud and subcloud layers will become uncoupled.

A suitable closure condition would again be that the negative areas on the θ_v diagram be a small fraction of the positive areas. This fixes T′ and ω_e and (conceptually) solves the time-dependent problem (see Section 4f).

Stage and Businger (1981a,b) have an extensive discussion of the closure problem for unsteady stratocumulus layers. They partition the $\overline{\omega'\theta_v'}$ flux into separate components (due to surface heating; cloud-top radiational cooling; cloud-top entrainment) before applying a closure. To the extent that our circulation model is valid, this seems unsound. The entrainment and radiative processes occur together at cloud top (see Section 5a) and the modified air sinks in the descending branch. The circulation as a whole has a CAPE, with distinct positive and negative regions, but in a circulation one cannot physically separate a contribution from the ascending air from the surface, from the descending air contribution; nor can one separate the buoyancy of the descending air into contributions from cloud-top mixing and radiation. This is discussed more extensively in the next section.

5. The role of cloud-top radiative cooling

a. Can cloud-top processes be partitioned?

This paper has constructed a circulation model with cloud-top radiation playing a role that has been the subject of some dispute (Schubert *et al.*, 1979a; Kahn and Businger, 1979; Deardorff and Businger, 1980; Deardorff, 1981; Lilly and Schubert, 1980; Stage and Businger, 1981a,b; Brost *et al.*, 1982b). In the model presented here, radiation is *both* an entrainment process at cloud top and a mechanism for CAPE generation for the circulation in the stratocumulus layer. However, by assumption we have explicit "turbulence" on only one scale: that of the single cell circulation of undetermined horizontal scale. This is clearly a simplification, but we know little about the scale on which radiative cooling does generate circulations. It is possible that a single-cell circulation or a downward penetrative convection (radiatively induced) may have a significantly different thermodynamic structure. This single-cell model should be regarded as a tool for exploring this question by comparing the model SP structure with observations. Stage and Businger (1981b) distinguish between cooling *in* the mixed layer which leads to turbulent kinetic energy generation and then entrainment (weighted by a factor, $A \approx 0.2$) and cooling *above* the mixed layer which leads to direct entrainment, which is in comparison five times as efficient (Stage and Businger, p. 2240). They do this despite assuming (consistent with observational studies) that the radiative heat loss is concentrated in a very thin layer at cloud top. However, if we recognize that the cloud-top interface is both thin compared to the mixed layer as a whole and likely to be turbulent (turbulence generated either by buoyancy forces or shear production), then it seems questionable to make closure dependent on partitioning radiative cooling just above and just below a thin, turbulent interface.

The circulation model presented here specifically avoids this. The entrainment process and radiative cooling are presumed to occur *together* at a turbulent cloud-clear air interface near $\mathcal{P} \approx 0$. It could be regarded that we are assuming sufficient small-scale turbulence exists to mix the thin interface on a time scale significantly shorter than the circulation time scale (h_T/ω^*). This seems likely. It then follows that air that approaches and leaves this interface has been modified by both processes. Although the SP analysis permits the conceptual partitioning of the cloud-top changes into a mixing process and radiative cooling, it also shows that thermodynamically it is irrelevant to the energetics of the circulation which happens first, provided they occur simultaneously at an interface which is thin compared with the overall depth of the mixed layer (or cloud layer). In contrast, Stage and Businger (1981b) partition the radiative and entrainment flux contributions to the turbulent kinetic energy budget.

There is some question whether one can use the same entrainment closure parameter to cover the whole range of possible stratocumulus circulations. We have shown that the unsteady case is somewhat more complex than the steady-state case. Nevertheless, we have also shown that direct entrainment by radiation and the turbulent kinetic energy budget can validly be treated as part of the same process using cloud-top radiation and a circulation model, whether the layer is in a steady state or not. Observational studies of SP structure can provide bulk estimates of entrainment and KE dissipation for different cases [e.g., using (17)].

b. Cloud-top versus distributed radiative divergence

Another aspect of this dispute has been the relative roles of radiative divergence localized at cloud top or

distributed through the mixed layer. Still ignoring the question of the horizontal scale of the circulations generated, a comparison can be made of the mean structural differences between a stratocumulus layer with cloud-top radiative divergence and a hypothetical case of uniform radiative cooling in the mixed layer, corresponding to the same overall radiative flux divergence. There are flux differences between these two cases which can be readily understood using an SP circulation diagram.

Fig. 9 compares the two cases for a layer in a steady state (and constant depth) with identical surface and cloud-top parameters, ω_0, **0**, ω_T, **T**. The modification of **T** to **T′** by **R** and subsequent steady-state mixing line structure **0MT′** was discussed in Section 2c.

(i) Distributed radiative cooling

If the same radiative divergence is distributed through the mixed layer and the layer is in a steady state, then there is a convective flux gradient with height which balances the radiative cooling. Diagrammatically the mixed-layer SP trend due to the flux divergence convection is **ME** in Fig. 9, which is just sufficient to balance the radiative cooling. Formally for a steady-state layer, $\omega_e = \omega_T$ and

$$0 = gh_T d\mathbf{M}/dt$$

$$= \omega_0(\mathbf{0} - \mathbf{M}) - \omega_e(\mathbf{M} - \mathbf{T}) + g\mathbf{R}, \quad (26)$$

$$0 = (\omega_e + \omega_0)(\mathbf{E} - \mathbf{M}) + g\mathbf{R}, \quad (27)$$

$$\therefore (\mathbf{M} - \mathbf{E}) = g\mathbf{R}/(\omega_0 + \omega_e). \quad (28)$$

The vectors **ME**, **TT′** are both parallel to **R** (which is along a line of constant q_s) and their magnitudes are in the ratio $\omega_e/(\omega_e + \omega_0)$, as is clear from the geometry of Fig. 9.

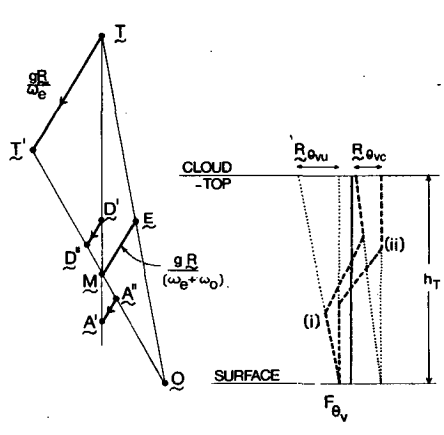

FIG. 9. Comparison of SP structure and θ_v fluxes (heavy dashed lines) for radiative flux difference (**R**): case (i), uniform distribution of radiative cooling through mixed layer with height-dependent internal circulation **A″A′** and **D″D′**; case (ii), cloud-top cooling with internal mixing line structure **0A″D″T′**.

Thus we see that distributed radiation gives a convective structure with SP's not on a mixing line. The convective circulation paths are those of the unsteady model (Section 4a), although the physical interpretation now shifts because the mixed layer is now in a steady state due to radiational cooling. The trend **A″A′** is now associated with the radiative cooling as air descends from surface to cloud top, where it mixes with air with SP at **T** to give **D′**, and then cools radiatively **D′D″** as it sinks in the descending branch. If the radiative flux divergence is uniform, then the change of SP with height is also uniform. The convective fluxes change correspondingly above the surface. Fig. 9 shows the θ_v flux distribution for cloud-top radiative divergence [case (ii): no height dependence] and distributed radiative cooling [case (i)], corresponding to the change of SP with height from **A″D″** to **A′D′** in Fig. 9. The net flux change by cloud-top height is related to **R** as shown. Correspondingly, the convective θ_L flux changes simply by R_θ from bottom to top of the layer.

If **0T′** satisfied some closure criteria on CAPE [Eq. (17)] relating the positive and negative areas on the θ_v flux diagram [case (ii)], it is clear that the circulation has markedly reduced CAPE if the cloud layer thins so that the radiative flux divergence becomes distributed through the layer [case (i)]. We would expect the cloud layer entrainment velocity ω_e to decrease and the mixed layer to become shallower as it adjusts to find a new ω_T, h_T where the closure condition (17) is again satisfied.

(ii) Cloud-top radiative cooling

The Fig. 9 flux diagram summarizes the θ_v flux structure correspondingly to this steady-state case (ii). At the risk of confusion, the SP circulation paths in Fig. 9 can be given a different interpretation for the case of localized cloud-top radiative divergence. In this case, most of the mixed layer has SP's **A″**, **D″** on the mixing line except *just below* cloud top, where the ascending air rapidly cools radiatively **A″** to **A′**, mixes with cloud-top air **T** to give **D′**, which then rapidly cools to **D″** as it leaves the interface. This is entirely equivalent to the cooling of subsiding air **TT′** before mixing.

This interpretation of Fig. 9 shows that if the cloud-top radiative process is included, then the criteria for cloud-top entrainment instability is more appropriate that **MT** (rather than **A″T**) have a slope to the left of the θ_{vc} (or θ_{ESV}) isopleth. Using (10a) and (8′) gives

$$(\mathbf{M} - \mathbf{T}) = \frac{\omega_0(\mathbf{0} - \mathbf{T}) + g\mathbf{R}}{\omega_0 + \omega_e}$$

$$= (\mathbf{E} - \mathbf{T}) + (\mathbf{M} - \mathbf{E}), \quad (29)$$

with $\omega_e = \omega_T$ in the steady-state case. Eq. (29) expresses the slope of **MT** in terms of external parameters.

We conclude that distributed radiation will reduce the layer instability and entrainment (ω_T in the steady state), as well as change the internal thermodynamic structure from a mixing line structure, and observational studies should be used to draw further inferences. However, the mixed layer circulation model remains an extremely useful and concise tool to properly define closure conditions. The SP circulation diagram can clearly be used to model intermediate cases where there is partial penetration of the radiative cooling into the mixed layer in terms of the radiative change of SP with height on A″A′ and D″D′.

6. Closing remarks

This paper has explored the thermodynamics of steady-state and unsteady mixed stratocumulus layers using saturation point diagrams and a circulation model. Many aspects of the analysis apply as a simpler case to dry mixed layers, and will be discussed elsewhere. Our conclusions fall into three main categories: those related to the usefulness of the SP method, some more specific to modeling mixed stratocumulus layers and some to the observational study of stratocumulus. Finally, we summarize our conclusions relating to the circulations in stratocumulus layers.

a. Usefulness of SP diagrams and budgets

Most of this paper has been concerned with the conceptual use of the saturation point in budget methods and on thermodynamic diagrams. In summary:

1) The SP notation concisely represents atmospheric thermodynamic budgets of θ_L, θ_E, θ_v and total water in a single diagram.

2) SP vector diagrams were used to depict cloud-top and surface fluxes as mixing processes, to formulate all layer fluxes as the product of a characteristic velocity and SP differences, to interrelate fluxes and mean layer structure, to couple convective and radiative fluxes, to depict the time-dependent budget, to depict mixed-layer circulation and relate Eulerian and Lagrangian flux descriptions for the time-dependent layer and to formulate closure conditions on circulation energetics.

3) Appendix B extends the definition of θ_v for cloudy processes on a thermodynamic diagram.

b. Modeling stratocumulus layers

The paper has developed a formal structure for modeling stratocumulus layers using a single-cell circulation model and SP methods. We noted:

1) Steady-state layers attain a mixing line thermodynamic structure. In unsteady layers, the deviation from this structure is related to flux gradients within the layer.

2) Simple parameterizations exist for the surface fluxes in a steady-state layer in terms of surface and cloud-top parameters.

3) Radiative cooling can act simultaneously as a cloud-top entrainment process as well as drive a convective circulation.

c. Observational studies of stratocumulus

Several aspects of the analysis have specific relevance to observational studies of stratocumulus, specifically:

1) The relationship between thermodynamic structure, boundary and internal fluxes for both steady-state and unsteady mixed layers (Figs. 2, 3 and 5).

2) The relationship between circulation mass flux and cloud base heights for ascending and descending branches (Fig. 2).

3) The relationship between circulation mass flux and the gradients with height of the thermodynamic parameters in ascending and descending branches for unsteady layers (Figs. 7 and 8).

4) The use of SP diagrams to interrelate convective and radiative processes at cloud top and within the layer (Figs. 2 and 9).

5) The relationship beween the mean structure of the layer and closure conditions on the circulation energetics (Figs. 3 and 8).

d. Circulation dynamics of stratocumulus

From a bulk viewpoint it seems that horizontally homogeneous stratocumulus layers fall into two classes:

1) Radiatively driven steady-state layers (Sections 2 and 3). These are typified by the cold ocean case (Sections 3a,b) where the surface buoyancy flux is small compared to the radiative flux divergence at cloud top. The main thermal balance is at cloud top. The radiative cooling drives entrainment by cooling air as it sinks through the cloud-top inversion and is mixed by small-scale turbulence at cloud top; and it drives the stratocumulus circulation by making cloudy mixtures negatively buoyant as they descend from cloud top. This CAPE drives a marginally indirect circulation below cloud base and transports water vapor from the surface. This type of radiatively driven circulation may also be relevant to the dynamics of stratocumulus layers in the middle atmosphere which are not coupled to the surface.

2) Unsteady layers driven by surface fluxes and cloud-top radiative cooling. These are typified by advection of cold air over a warm ocean, where the surface heat flux is upward, large and comparable to the cloud-top radiative flux difference. The layer is not in a steady state but entrains rapidly as it warms up. The entrainment rate is larger than that in the preceding paragraph *d*1) (and the flux gradients correspondingly steeper) so that there are small regions of negative θ_v flux (below cloud base, and/or below cloud top). In this case en-

trainment and the circulation are driven by both radiative and surface fluxes.

It remains for observational studies to explore the usefulness of this simple saturation point circulation model in determining bulk entrainment and dissipation parameters for stratocumulus layers and as a parametric method.

Acknowledgments. This work was supported by the Atmospheric Sciences Section (Global Atmospheric Research Program) of the National Science Foundation under Grant ATM-8120444. I am grateful to one of the reviewers for improving the manuscript.

APPENDIX A

Flux of Saturation Pressure Difference

We consider the change of SL associated with corresponding changes of saturation level θ_{SL}, q_{SL}, where

$$\delta p_{SL} = \left(\frac{\partial p_{SL}}{\partial \theta_{SL}}\right)_{qSL} \delta\theta_{SL} + \left(\frac{\partial p_{SL}}{\partial q_{SL}}\right)_{\theta SL} \delta q_{SL}.$$

The differentials are just the inverse of the gradients of θ, q_s along lines of constant q_s, θ on a thermodynamic diagram, and over small pressure ranges we might approximate them by mean values: C_1, C_2. Dropping the SL subscripts on θ and q for brevity, we may regard perturbations p'_{SL} as linear combinations of perturbations θ', q'. Furthermore, perturbations in the layer will be closely hydrostatic, so that $\mathcal{P}' = p'_{SL}$. Hence we may write

$$F_{\mathcal{P}} = \overline{\omega'\mathcal{P}'} = \overline{\omega' p'_{SL}} = C_1 F_\theta + C_2 F_q, \qquad \text{(A1)}$$

and for the cloud-top radiative flux difference

$$R_{\mathcal{P}} = C_1 R_\theta. \qquad \text{(A2)}$$

APPENDIX B

θ_v Isopleths

For unsaturated air, using SP notation, the line of constant θ_{vu} is given by (Betts, 1982a)

$$\text{constant} = \theta_{vu}(p_{SL}) = \theta_{SL} + 0.61 q_{SL}. \qquad \text{(B1)}$$

The value of the constant is the value of θ as $q \to 0$. As q increases the derivation of the θ_{vu} isopleth from the dry adiabat increases (see Betts, 1982a). For cloudy air

$$\theta_{vc}(p, p_{SL}) = \theta(p)[1 + 0.61 q_s(p) - l(p, p_{SL})]. \qquad \text{(B2)}$$

Betts (1982a) showed how isopleths of θ_{vc} could be drawn on a thermodynamic diagram—they have slopes of ~0.9 of the slope $(\partial\theta/\partial p)$ of the moist adiabat.

Deardorff (1976, 1980a) showed how θ_{vc} *perturbations* can be expressed as linear combinations of *conserved* parameters. In SP notation

$$\delta\theta_{vc} = \eta_1 \delta\theta_{ESL} - \theta\delta q_{SL}, \qquad \text{(B3)}$$

where

$$\left.\begin{aligned} \eta_1 &\approx \theta(1 + 1.61\alpha)/(1 + L\alpha/C_pT)\theta_{ES} \\ \alpha &= Tdq_s/dT\,. \end{aligned}\right\} \qquad \text{(B4)}$$

Rearranging (B3) permits a definition of an isopleth of virtual θ_{ES}

$$0 = \delta\theta_{ESV} = \delta\theta_{ESL} - \theta_{ES}\delta q_{SL}/\eta_2, \qquad \text{(B5)}$$

where

$$\eta_2 = \frac{\theta_{ES}}{\theta}\eta_1.$$

These θ_{ESV} isopleths have the same slope as the θ_{vc} isopleths: 0.9 of the moist adiabat. Alternatively, we may write the slope as (Deardorff, 1980a)

$$\left(\frac{\partial\theta_{ESL}}{\partial q_{SL}}\right)_{\theta ESV} = \frac{\theta}{\eta_1} = \frac{\theta_{ES}}{\eta_2}.$$

Eq. (B5) can be formally integrated along a line of constant θ_{ESV} from p_0 to p to define a value of θ_{ESV} such that

$$\theta_{ESV} = \theta_{ES}(p_0) = \theta_{ES}(p) - \int_{p_0}^{p} \frac{\theta_{ES}}{\eta_2} dq_{SL}. \qquad \text{(B6)}$$

Here, η_2 is a strongly varying function of q_s (see Table 1) and must be evaluated numerically. Eq. (B6) defines an isopleth that deviates from the moist adiabat as q_s increases, analogous to the deviation of the θ_{vu} isopleth from the dry adiabat (B1). It can be labeled with the value of θ_{ES} at any p_0. If we let $p_0 \to 0$ (where $q_s \to 0$), we define

$$\theta'_{ESV} = \theta_{ES}(p) - \int_0^{q_s} \left(\frac{\theta_{ES}}{\eta_2}\right) dq_{SL}. \qquad \text{(B7)}$$

Conceptually this means that a parcel ascending until it has condensed its water content has a lower θ_v (higher density) than a parcel without the liquid water loading. To be consistent, the θ_{ES} should in this case not be that of the pseudo-adiabat, but the reversible water-saturation adiabat to allow for the additional thermal consequences of carrying the liquid water (and for some purposes, the reversible ice saturation adiabat). Alter-

TABLE 1. Variation of thermodynamic parameters with q_s at 900 mb (p variation is small).

	($g\ kg^{-1}$)			
q_s	5	10	15	20
α	0.10	0.19	0.28	0.37
$1/\eta_2$	1.64	2.05	2.35	2.59
$1 + 0.61\alpha$	1.06	1.12	1.17	1.23

natively, and perhaps more useful for shallow cloud problems, p_0 could be set at 1000 mb (or even cloud base) to define a different label

$$\theta_{ESV} = \theta_{ES}(p) + \int_{q_s}^{q_s(1000)} (\theta_{ES}/\eta_2) dq_{SL}. \quad \text{(B8)}$$

Over small ranges of q_s and p, the pseudo-adiabats can be used for θ_{ES} and, for some conceptual purpose, η_2 can also be taken as constant. We use (B8) in Fig. 10.

We can compare the buoyancy of parcels with different SP's by overlaying the field of θ_{vu} isopleths for unsaturated parcels and θ_{ESV} for cloudy parcels. Both sets of isopleths are unique functions of SP and can be regarded as density analogs of the θ, θ_{ES} isopleths on a thermodynamic diagram.

Each θ_{ESV} isopleth corresponds for each parcel pressure p to a specific value of θ_{vc}, that of the θ_{vu} isopleth which it intersects at p. As parcel pressure changes, θ_{ES}, θ_{ESV} do not change but θ, θ_{vc} of course do. Fig. 10 shows examples. While unsaturated, a parcel with SP at **A** has θ_{vu} = 304 K. If it ascends (moist) adiabatically to pressure p_2, θ_{vc} = 307.1 K; to p_3, θ_{vc} = 310.4 K, while retaining the same θ_{ESV}. The difference of θ_{vc} at constant pressure between **A** and **D** (while both are cloudy) increases as p decreases, primarily because of the change of η_1 in (B3).

By projecting parcel SP's using the two sets of isopleths to parcel pressure p (using θ_{vu} if $p > p_{SL}$, and θ_{vc} or θ_{ESV} for $p < p_{SL}$), one can compare the buoyancies of two parcels at changing pressure levels. At pressure p_1 in Fig. 10, parcels **A** and **D** have the same density as just saturated parcels (with SP's) at A_1, D_1 on the corresponding θ_{vu} isopleths; while at p_2, when **A** and **D** are cloudy, they have the same density as just saturated parcels at A_2, D_2 on the corresponding θ_{ESV} isopleths. For the circulation diagrams, where A and D are the SP's of ascending and descending branches, this means one can construct an area (shaded) on the tephigram which is still closely related to convective available potential energy. The differences $\delta\theta$, $\delta\theta_v$ between the just saturated pairs A_1D_1 or A_2D_2 satisfy

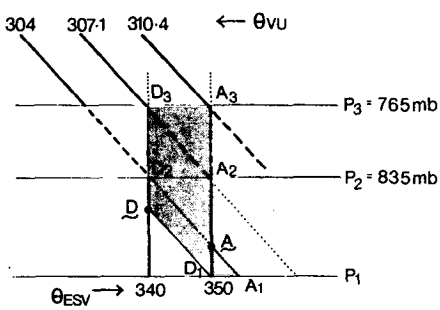

FIG. 10. θ_v isopleths for unsaturated air (θ_{vu}) and cloudy air (θ_{ESV}). Comparison of buoyancies (θ_v) at different pressures (p_1, p_2, p_3) for parcels with SP's at **A**,**D**. Shaded area is related to buoyancy integral.

$$\frac{\delta\theta_{vu}}{\delta\theta_{vu}} = \frac{\delta\theta}{\theta}(1 + 0.61\alpha).$$

Thus,

$$\text{CAPE} = \int g\frac{\delta\theta_v}{\theta_v}dz \approx (1 + 0.61\alpha)\int g\frac{\delta\theta}{\theta}dz.$$

The energy integral $\int g(\delta\theta/\theta)dz$ is proportional to an area on a tephigram. Hence, so is CAPE = $\int g(\delta\theta_v/\theta_v)dz$, provided the coefficient $(1 + 0.61\alpha)$ is sensibly constant over the area of integration. Table 1 shows the coefficient is near unity and increases slowly with q_s.

We use the notation $(\mathbf{A} - \mathbf{D})_{\theta_v}$ for the projection of the SP differences onto the θ_v isopleths. For cloudy parcels,

$$\delta\theta_v = (\mathbf{A} - \mathbf{D})_{\theta_{vc}},$$

and the buoyancy flux is

$$\overline{\omega'\theta'_{vc}} = \omega^*(\mathbf{A} - \mathbf{D})_{\theta_{vc}}.$$

This is entirely equivalent to the flux form of (B3) as used in Deardorff (1980a) and Randall (1980), i.e.,

$$\omega'\theta'_{vc} = \eta_1\overline{\omega'\theta'_{ES}} - \theta\overline{\omega'q'_T}. \quad \text{(B3')}$$

REFERENCES

Arakawa, A., and W. Schubert, 1974: Interaction of a cumulus cloud ensemble with the large-scale environment: Part I. *J. Atmos. Sci.*, **31**, 674–701.

Ball, F. K., 1960: Control of inversion height by surface heating. *Quart. J. Roy. Meteor. Soc.*, **86**, 264–273.

Betts, A. K., 1973: Non-precipitating convection and its parameterization. *Quart. J. Roy. Meteor. Soc.*, **99**, 178–196.

——, 1974: Further comments on "A comparison of the equivalent potential temperature and static energy." *J. Atmos. Sci.*, **31**, 1713–1715.

——, 1975: Parametric interpretation of trade-wind cumulus budget studies. *J. Atmos. Sci.*, **32**, 1934–1945.

——, 1976: Modeling subcloud layer structure and interaction with a shallow cumulus layer. *J. Atmos. Sci.*, **33**, 2363–2382.

——, 1978: Convection in the tropics. *Meteorology over the Tropical Oceans. Quart. J. Roy. Meteor. Soc.* (Suppl.), 105–132.

——, 1982a: Saturation point analysis of moist convective overturning. *J. Atmos. Sci.*, **39**, 1484–1505.

——, 1982b: Cloud thermodynamic models in saturation point coordinates. *J. Atmos. Sci.*, **39**, 2182–2191.

Brost, R. A., D. H. Lenschow and J. C. Wyngaard, 1982a: Marine stratocumulus layers. Part I: Mean conditions. *J. Atmos. Sci.*, **39**, 800–817.

——, J. C. Wyngaard and D. H. Lenschow, 1982b: Marine stratocumulus layers. Part II: Turbulence budgets. *J. Atmos. Sci.*, **39**, 818–836.

Carson, D. J., 1973: The development of a dry inversion-capped convectively unstable boundary layer. *Quart. J. Roy. Meteor. Soc.*, **99**, 450–467.

Caughey, S. J., B. A. Crease and W. T. Roach, 1982: A field study of nocturnal stratocumulus: II: Turbulence structure and entrainment. *Quart. J. Roy. Meteor. Soc.*, **108**, 125–144.

Deardorff, J. W., 1976: On the entrainment rate of a stratocumulus topped mixed layer. *Quart. J. Roy. Meteor. Soc.*, **102**, 563–582.

——, 1980a: Cloud-top entrainment instability. *J. Atmos. Sci.*, **37**, 131–147.

——, 1980b: Stratocumulus mixed layers derived from a three-dimensional model. *Bound.-Layer Meteor.*, **18**, 495–527.

——, 1981: On the distribution of mean radiative cooling at the top of a stratocumulus-capped mixed layer. *Quart. J. Roy. Meteor. Soc.*, **107**, 191–202.

——, and J. A. Businger, 1980: Comments on "Marine stratocumulus convection. Part I: Governing equations and horizontally homogenous solutions." *J. Atmos. Sci.*, **37**, 481–482.

Greenhut, G. K., and S. J. S. Khalsa, 1982: Updraft and downdraft events in the atmospheric boundary layer over the equatorial Pacific Ocean. *J. Atmos. Sci.*, **39**, 1803–1818.

Kahn, P. H., and J. A. Businger, 1979: The effect of radiative flux divergence on entrainment of a saturated convective boundary layer. *Quart. J. Roy. Meteor. Soc.*, **105**, 303–306.

Kraus, H., and E. Schaller, 1978: Steady state characteristics of inversions capping a well-mixed planetary boundary layer. *Bound.-Layer Meteor.*, **14**, 83–104.

Lilly, D. K., 1968: Models of cloud-topped mixed layers under a strong inversion. *Quart. J. Roy. Meteor. Soc.*, **94**, 292–309.

——, and W. H. Schubert, 1980: The effects of radiative cooling in a cloud-topped mixed layer. *J. Atmos. Sci.*, **37**, 482–487.

Mahrt, L., and J. Paumier, 1982: Cloud-top entrainment instability observed in AMTEX. *J. Atmos. Sci.*, **39**, 622–634.

Manins, P. C., and J. S. Turner, 1978: The relationship between flux ratio and energy ratio in convectively mixed layers. *Quart. J. Roy. Meteor. Soc.*, **104**, 39–44.

Moeng, C-H., and A. Arakawa, 1980: A numerical study of a marine subtropical stratus cloud layer and its stability. *J. Atmos. Sci.*, **37**, 2661–2676.

Nicholls, S., and M. A. LeMone, 1980: The fair weather boundary layer in GATE: The relationship of subcloud fluxes and structure to the distribution and enhancement of cumulus clouds. *J. Atmos. Sci.*, **37**, 2051–2067.

Randall, D. A., 1980: Conditional instability of the first kind upside-down. *J. Atmos. Sci.*, **37**, 125–130.

Roach, W. T., R. Brown, S. J. Caughey, B. A. Crease and A. Slingo, 1982: A field study of nocturnal stratocumulus: I. Mean structure and budgets. *Quart. J. Roy. Meteor. Soc.*, **108**, 103–124.

Schubert, W. H., 1976: Experiments with Lilly's cloud-topped mixed layer model. *J. Atmos. Sci.*, **33**, 436–446.

——, J. S. Wakefield, E. J. Steiner and S. K. Cox, 1979a: Marine stratocumulus convection. Part 1: Governing equations and horizontally homogeneous solutions. *J. Atmos. Sci.*, **36**, 1286–1307.

——, ——, —— and ——, 1979b: Marine stratocumulus convection. Part II: Horizontally inhomogeneous solutions. *J. Atmos. Sci.*, **36**, 1308–1324.

Slingo, A., S. Nichols and J. Schmetz, 1982: Aircraft observations of marine stratocumulus during JASIN. *Quart. J. Roy. Meteor. Soc.*, **108**, 833–856.

Stage, S. A., and J. A. Businger, 1981a: A model for entrainment into a cloud-topped boundary layer. Part I: Model description and application to a cold air outbreak. *J. Atmos. Sci.*, **38**, 2213–2229.

——, and ——, 1981b: A model for entrainment into a cloud-topped boundary layer. Part II: Discussion of model behavior and comparison with other models. *J. Atmos. Sci.*, **38**, 2230–2242.

Tennekes, H., 1973: A model for the dynamics of the inversion above a convective boundary layer. *J. Atmos. Sci.*, **30**, 558–567.

Yanai, M., S. Esbenson and J. Chu, 1973: Determination of bulk properties of tropical cloud clusters from large-scale heat and moisture budgets. *J. Atmos. Sci.*, **31**, 1297–1307.